CROMER, D. T. & LIBERMAN, D. (1970). *J. Chem. Phys.* **53**, 1891–1898.
DELAPLANE, R. G. & IBERS, J. A. (1969). *Acta Cryst.* B**25**, 2423–2437.
DESMEULES, P. J. & ALLEN, L. C. (1980). To be published.
DREYFUS, M. & PULLMAN, A. (1970). *Theor. Chim. Acta*, **19**, 20–37.
FELD, R. & LEHMANN, M. S. (1979). Unpublished results.
GRIFFIN, J. F. & COPPENS, P. (1975). *J. Am. Chem. Soc.* **97**, 3496–3505.
HAMILTON, W. C. & IBERS, J. A. (1968). *Hydrogen Bonding in Solids*. New York: Benjamin.
HANSEN, N. K. & COPPENS, P. (1978). *Acta Cryst.* A**34**, 909–921.
HAREL, M. & HIRSHFELD, F. L. (1975). *Acta Cryst.* B**31**, 162–172.
*International Tables for X-ray Crystallography* (1974). Vol. IV. Birmingham: Kynoch Press.
JOHANSEN, H. (1979). *Acta Cryst.* A**35**, 319–325.
KOLLMAN, P. A. (1977). *Applications of Electron Structure Theory*, edited by H. F. SCHAEFER, pp. 109–152. New York: Plenum.
KOLLMAN, P. A. & ALLEN, L. C. (1972). *J. Am. Chem. Soc.* **94**, 6101–6107.
KVICK, Å., KOETZLE, T. F. & STEVENS, E. D. (1979). *J. Chem. Phys.* **71**, 173–179.
KVICK, Å., THOMAS, R. & KOETZLE, T. F. (1976). *Acta Cryst.* B**32**, 224–231.
MCCANDLISH, L. E., STOUT, G. H. & ANDREWS, L. C. (1975). *Acta Cryst.* A**31**, 245–249.
MCMULLEN, R. K. & KOETZLE, T. F. (1979). Private communication.
OLOVSSON, G., KVICK, Å., LEHMANN, M. & OLOVSSON, I. (1980). To be published.
OLOVSSON, I. (1980). *NATO Advanced Study Institute. Electronic & Magnetic Distributions in Molecules and Crystals*, edited by P. BECKER. New York: Plenum.
REES, B. (1976). *Acta Cryst.* A**32**, 483–488.
SABINE, T. M., COX, G. W. & CRAVEN, B. M. (1969). *Acta Cryst.* B**25**, 2437–2441.
SCHLEMPER, E. O. & HSU, B. (1978). *Am. Crystallogr. Assoc. Abstr.* **6**, 15.
SMITH, V. H. (1977). *Phys. Scr.* **15**, 147–162.
STEVENS, E. D. (1977). *Acta Cryst.* A**33**, 580–584.
STEVENS, E. D. (1978). *Acta Cryst.* B**34**, 544–551.
STEVENS, E. D. (1980). *Acta Cryst.* B**36**, 1876–1886.
STEVENS, E. D. & COPPENS, P. (1977). *J. Cryst. Mol. Struct.* **7**, 251–255.
STEVENS, E. D., LEHMANN, M. S. & COPPENS, P. (1977). *J. Am. Chem. Soc.* **99**, 2829–2831.
STEWART, R. F. (1976). *Acta Cryst.* A**32**, 565–574.
STEWART, R. F., DAVIDSON, E. R. & SIMPSON, W. T. (1965). *J. Chem. Phys.* **42**, 3175–3187.
TAKUSAGAWA, F. & KOETZLE, T. F. (1979). *Acta Cryst.* B**35**, 867–877.
TAYLOR, J. C. & SABINE, T. M. (1972). *Acta Cryst.* B**28**, 3340–3351.
TELLGREN, R., THOMAS, J. O. & OLOVSSON, I. (1977). *Acta Cryst.* B**33**, 3500–3504.
THOMAS, J. O. (1978). *Acta Cryst.* A**34**, 819–823.
THOMAS, J. O., TELLGREN, R. & ALMLÖF, J. (1975). *Acta Cryst.* B**31**, 1946–1955.
WAL, H. VAN DER (1979). Thesis, Univ. of Groningen, Groningen, The Netherlands.
WANG, Y., BLESSING, R. H., ROSS, F. K. & COPPENS, P. (1976). *Acta Cryst.* B**32**, 572–578.
YAMABE, S. & MOROKUMA, K. (1975). *J. Am. Chem. Soc.* **97**, 4458–4465.

*Acta Cryst.* (1980). B**36**, 1876–1886

# Comparison of Theoretical and Experimental Electron Density Distributions of Oxalic Acid Dihydrate

BY E. D. STEVENS

*Chemistry Department, State University of New York at Buffalo, Buffalo, New York* 14214, *USA*

(*Received* 13 *August* 1979; *accepted* 24 *March* 1980)

## Abstract

Thermally smeared theoretical electron density distributions of the oxalic acid molecule are compared with the experimental density of α-oxalic acid dihydrate obtained from high-resolution X-ray diffraction measurements at 100 K. Theoretical densities are calculated from extended-basis-set and 4-31G wavefunctions and smeared using experimental rigid-body translational and librational thermal parameters. Over much of the molecule, the agreement between the experimental and etended-basis-set theoretical density is within twice the estimated standard deviation of the experimental density. The largest significant differences are attributed to the effects of hydrogen bonding neglected in the theoretical calculations. The agreement between the experimental and dynamic 4-31G theoretical density is significantly worse. Comparison of static multipole model densities with static theoretical densities indicates that sharp features of the

0567-7408/80/081876-11$01.00 

static density are not recovered by deconvolution. Extended-basis-set static theoretical densities calculated for a water dimer with geometry corresponding to the short hydrogen bond in oxalic acid are in agreement with the experimental density along the hydrogen bond but fail to predict the perturbation experimentally observed in the density of the acceptor water molecule.

## Introduction

In recent years, improvements in experimental design and low-temperature techniques have increased the accuracy of experimental measurements of the electron density distribution in crystals by X-ray diffraction. At the same time, improved computational methods and computing capacity have led to an improvement in the quality of theoretical densities. For a molecular crystal consisting of only light atoms, both experimental and theoretical densities may be obtained with an accuracy suitable for detailed and meaningful quantitative comparison. In addition to providing information on the electronic structure of the molecule, comparison between theory and experiment provides a measure of the reliability of the method and reveals deficiencies in both theory and experiment.

The most significant problem in direct comparison of experimental and theoretical charge densities is accounting for the smearing of the experimental density by thermal motion. Whether it is better to apply thermal smearing to the theoretical density or deconvolute thermal motion from the experimental density has not been resolved (Coppens & Stevens, 1977). In several previous studies (see for example Stevens, Rys & Coppens, 1977*a*, 1978; Helmholdt & Vos, 1977; Irngartinger, Hase, Schulte & Schweig, 1977), experimental densities have been compared with dynamic theoretical electron distributions. In some recent studies, however, static theoretical densities have been compared with experimental static model densities (Dietrich & Scheringer, 1978; Scheringer, Mullen & Hellner, 1978; Scheringer, Kutoglu, Hellner, Hase, Schulte & Schweig, 1978).

Although a number of studies have shown that static theoretical densities converge slowly with increasing basis-set size and that extended basis sets including polarization functions are required to approach the Hartree–Fock limit (Bader, 1975; Cade, 1972), the effect of thermal smearing on the rate of convergence of dynamic densities has not been investigated. A related question is whether the accuracy of present experiments is sufficient to distinguish between dynamic densities of minimal basis set, double-$\zeta$, or near-Hartree–Fock quality (Hase, Reitz & Schweig, 1976; Hase, Schulte & Schweig, 1977).

We report here detailed comparisons of the experimental electron density distribution of $\alpha$-oxalic acid dihydrate at 100 K (Stevens & Coppens, 1980) with dynamic theoretical densities calculated with two different basis sets. Since the theoretical calculations correspond to isolated oxalic acid molecules while the experiment yields the electron distribution within the crystal, differences due to the effects of intermolecular interactions in the solid will contribute to the differences between theoretical and experimental densities.

## Computational methods

### *Theoretical densities*

Theoretical molecular orbital wavefunctions have been calculated for the oxalic acid molecule by *ab initio* self-consistent-field methods (Roothaan, 1951) using the program *HONDO* (Dupuis, Rys & King, 1976; Dupuis & King, 1977) and an extended basis of Gaussian orbitals. To test the sensitivity of the results to basis-set size, calculations have been performed with an extended basis set (EBS) including *d* functions (Pople & Binkley, 1975) and with the popular 4-31G basis set (Ditchfield, Hehre & Pople, 1971). The extended basis set consisted of (11,5,1/6,1) primative Gaussians contracted to a $\langle 4,3,1/4,1\rangle$ set, while the 4-31G basis consisted of (8,4,0/4,0) primatives contracted to a $\langle 3,2,0/2,0\rangle$ set.

The geometry of the oxalic acid molecule used for the calculation was obtained from bond distances and angles determined by neutron diffraction at room temperature (Coppens & Sabine, 1969). The coordinates of the atomic centers are listed in Table 1. The atom numbering scheme is the same as that used for the experimental studies (Coppens & Sabine, 1969; Stevens & Coppens, 1980).

The total energy for the molecule calculated for the SCF wavefunction with the extended basis set, $E = -376{\cdot}4458$ a.u., is slightly higher than the lowest energy of $-376{\cdot}4864$ a.u. reported by Johansen (1979). Calculation with the 4-31G basis yields a total energy of $-375{\cdot}7790$ a.u.

In order to display the small changes that occur in atomic electron density distributions from chemical

Table 1. *Atomic coordinates (molecular system) used in theoretical calculations on oxalic acid (in atomic units)*

| | *x* | *y* | *z* |
|---|---|---|---|
| C(1) | 1·4541723 | 0·0 | 0·0 |
| O(1) | 2·3759985 | 2·2588332 | 0·0 |
| O(2) | 2·6367857 | −1·9526917 | 0·0 |
| H(1) | 4·3241548 | 2·2792427 | 0·0 |
| C(1′) | −1·4541723 | 0·0 | 0·0 |
| O(1′) | −2·3759985 | −2·2588332 | 0·0 |
| O(2′) | −2·6367857 | 1·9526917 | 0·0 |
| H(1′) | −4·3241548 | −2·2792427 | 0·0 |

Table 2. *Atomic coordinates used in theoretical calculations of the water dimer (in atomic units)*

| | *x* | *y* | *z* |
|---|---|---|---|
| O(1) | 0·0 | 0·0 | 0·0 |
| O(2) | 4·6988947 | 0·0 | 0·0 |
| H(1) | −0·7433978 | 0·8226284 | −1·4605197 |
| H(2) | −0·7433978 | 0·8226284 | 1·4605197 |
| H(3) | 2·6749589 | 0·0 | 0·0 |
| H(4) | 5·1974888 | −1·8183636 | 0·0 |

bonding, the deformation density, $\Delta\rho = \rho_{\text{molecule}} - \rho_{\text{atoms}}$, is plotted where $\rho_{\text{molecule}}$ is the one-electron density distribution calculated for the molecular wavefunction and $\rho_{\text{atoms}}$ is the superposition of isolated, spherically averaged atomic densities. To avoid basis-set truncation effects, the ground-state atomic densities are calculated from open-shell restricted Hartree–Fock wavefunctions (Roos, Salez, Viellard & Clementi, 1968), using the same basis set. The extended atomic basis sets for carbon and oxygen include an extra 3*s* function generated from the EBS representation of *d* functions by six Gaussian-type functions.

Theoretical deformation densities of the water dimer, $(H_2O)_2$, in the *trans* linear geometry have also been calculated using the extended basis set. Atomic coordinates are listed in Table 2.

### *Thermal smearing*

Experimental electron density distributions are averaged over the thermal motion of the atoms in the crystal. To compare theoretical density distributions directly with experimental results, the effect of thermal motion must be taken into account. This may be done by either deconvolution of thermal motion from the experimental density or application of thermal smearing to the theoretical density (Coppens & Stevens, 1977). Both techniques are considered here.

The proper treatment of thermal motion in the Born–Oppenheimer approximation involves calculation of the wavefunction at all possible nuclear positions and taking the thermally weighted average of the densities over all vibrational modes. However, since for a molecular crystal the internal modes of vibration have amplitudes which are normally much smaller than the external modes, the dynamic theoretical density may be calculated to a good approximation from the static density at a single geometry by convolution with the rigid-body thermal motions (Stevens, Rys & Coppens, 1977*b*).

Values for the rigid-body translational and librational thermal-motion tensors (Schomaker & Trueblood, 1968) have been obtained for the oxalic acid molecule by a fit to the individual atomic thermal parameters experimentally determined at 100 K (refinement II; Stevens & Coppens, 1980). Since the molecule sits at an inversion center in the crystal, no screw tensor occurs. The fit of the rigid-body thermal parameters to the individual atomic parameters is generally good (average difference, 0·001 Å$^2$) except for H(1) which shows an excess thermal motion of 0·007 Å$^2$ along the H(1)–O(1) bond compared to the rigid-body model. The thermal parameters used to smear the theoretical density distribution are listed in Table 3 with the transformation matrices relating the molecular, crystal and inertial frames of reference.

Table 3. *Rigid-body thermal parameters of oxalic acid used to calculate the dynamic theoretical density*

Translation tensor (Å$^2$, relative to inertial axes)

| | | |
|---|---|---|
| 0·00749 (34) | 0·00040 (33) | 0·00035 (37) |
| | 0·00766 (45) | −0·00021 (46) |
| | | 0·01199 (68) |

Libration tensor (rad$^2$, relative to inertial axes)

| | | |
|---|---|---|
| 0·00629 (71) | 0·00032 (19) | 0·00017 (25) |
| | 0·00154 (26) | 0·00004 (15) |
| | | 0·00146 (13) |

Transformation from molecular to crystal coordinates

| | | |
|---|---|---|
| −0·030806 | 0·070675 | −0·046813 |
| 0·040328 | −0·067873 | −0·129006 |
| 0·035627 | 0·028842 | −0·004037 |

Transformation from crystal to inertial coordinates

| | | |
|---|---|---|
| −2·99427 | 0·73718 | 11·31778 |
| −4·27517 | 1·67984 | −3·78009 |
| −3·15149 | −2·97920 | 0·66908 |

The dynamic theoretical density is calculated by placing the static oxalic acid density at each of the molecular sites in the monoclinic unit cell of oxalic acid dihydrate and then evaluating analytically the Fourier transform of the density for each scattering vector **s** corresponding to an experimental measurement. After multiplication of the theoretical structure factors by the rigid-body temperature factor, the smeared density is obtained by an inverse Fourier transform. Since the theoretical structure factors are calculated only to the limit of the experimental measurements, series-termination effects will be included in the theoretical density to the same extent as in the experiment. The resulting density distribution of the crystal is the superposition of smeared, isolated molecular densities (with water molecules excluded).

### *Stereographic projections*

In addition to calculating the theoretical density in planar sections, the non-bonding density around the oxygen atoms has been calculated in stereographic projection (Stevens & Coppens, 1980). The deformation density on the surface of hemispheres of radius 0·3 Å and centered on the oxygen atoms has been

projected onto the planes perpendicular to the CO bonds. Stereographic projections are especially useful for displaying the atomic hybridization and angular orientation of the lone-pair density features.

*Experimental densities*

The experimental electron density distribution of α-oxalic acid dihydrate has been determined from high-resolution single-crystal X-ray diffraction measurements at 100 K. Details of the experiment are described by Stevens & Coppens (1980). The (dynamic) deformation density has been calculated by subtracting isolated spherical Hartree–Fock atomic densities with positional and thermal parameters for carbon and oxygen determined from high-order X-ray data and hydrogen parameters determined by neutron diffraction (Feld & Lehmann, 1979).

The estimated standard deviation of the experimental deformation density is relatively constant with an average value of 0·02 e/Å$^3$ at a general position in the crystal and 0·03 e/Å$^3$ at the inversion center in the C–C bond. Near the atom centers, however, errors in the refined positional and thermal parameters and X-ray scale factor result in an estimated error which rapidly increases to more than 0·9 e/Å$^3$ at the carbon and nitrogen nuclei.

*Double difference densities*

To facilitate detailed comparison of the theoretical and experimental deformation densities, a second-order difference function defined by

$$\Delta(\Delta\rho) = \Delta\rho_{\text{exp}} - \Delta\rho_{\text{theory, dynamic}}$$

has been calculated. Since the same reference state (a superposition of spherical atom densities) has been used for both $\Delta\rho_{\text{exp}}$ and $\Delta\rho_{\text{theory, dynamic}}$, except for slight differences in positions, thermal parameters and atomic densities, the function $\Delta(\Delta\rho)$ is essentially equivalent to the difference between the total experimental electron density in the crystal and the total smeared density of the molecule.

Positive regions of $\Delta(\Delta\rho)$ indicate an excess of charge in the experimental density relative to the theoretical calculation. The significance of deviations of $\Delta(\Delta\rho)$ from zero must be judged by consulting the error distribution map.

The deviation of the bond peaks from cylindrical symmetry has been plotted in another double difference density, $\rho_{L\neq 0} = \Delta\rho - \Delta\rho(90°)$, where the cylindrical component is removed by rotating about the bond by 90° (Stevens & Coppens, 1980). In addition, *mm* symmetry is imposed by averaging.

## Results

*Oxalic acid*

The static deformation density of the extended-basis-set wavefunction calculated in the plane of the oxalic acid molecule is plotted in Fig. 1(*a*). For comparison with experiment, contour maps are plotted here at equal intervals. When the same density is plotted on a logarithmic scale, the map is entirely superimposable with the density calculated by Johansen (1979). The deformation calculated using the smaller 4-31G basis is plotted in Fig. 1(*b*). Both maps show peaks in each of the covalent bonds and in the

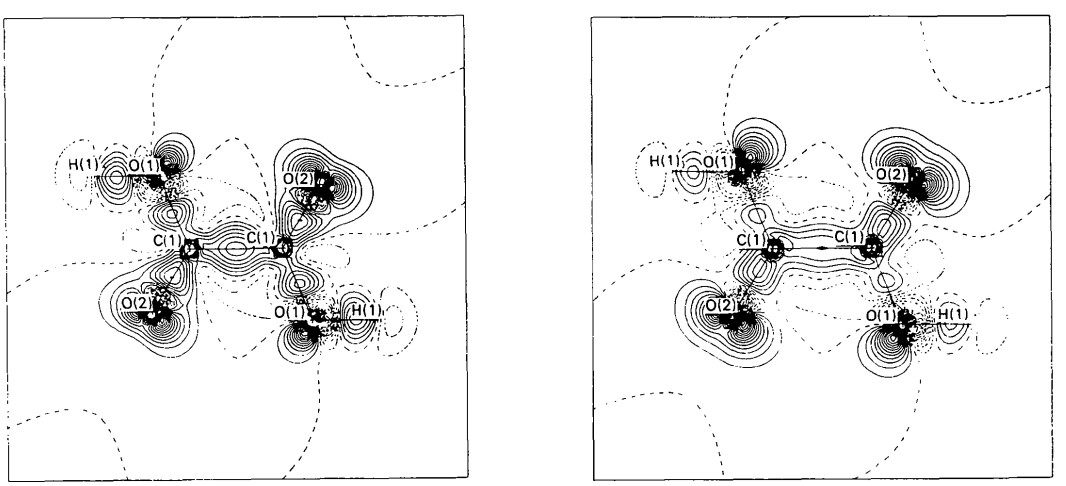


(*a*) (*b*)

Fig. 1. (*a*) Static EBS theoretical deformation density calculated in the plane of the oxalic acid molecule. Contours are plotted at intervals of 0·10 e/Å$^3$ with the zero and negative contours dashed. (*b*) Static theoretical density calculated with the 4-31G basis set. Contours as in (*a*).

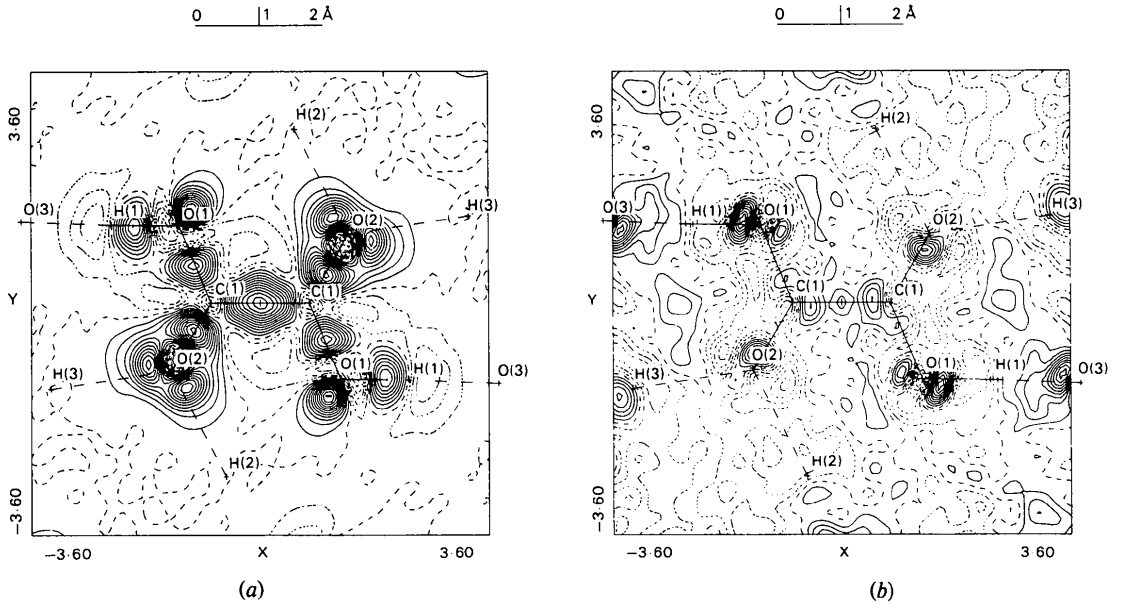


Fig. 2. (*a*) Dynamic EBS theoretical deformation density of oxalic acid. Contours at 0·05 e/Å$^3$ with zero and negative contours dashed. (*b*) Difference between experimental and dynamic EBS theoretical deformation densities in the molecular plane. Contours as in (*a*).

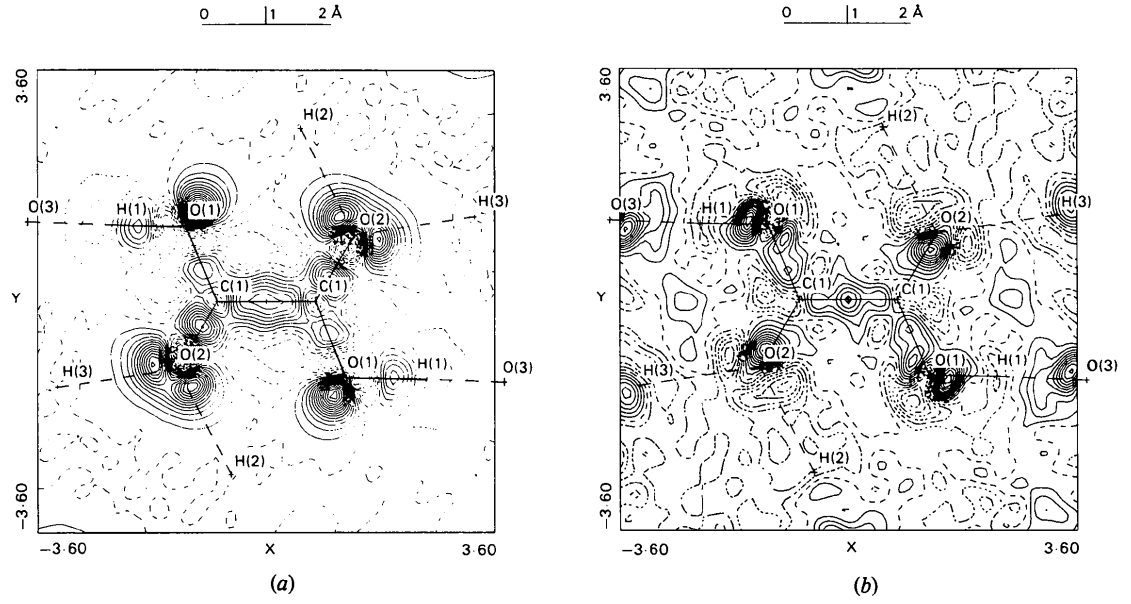


Fig. 3. (*a*) Dynamic 4-31G theoretical deformation density of oxalic acid. Contours as in Fig. 2(*a*). (*b*) Difference between experimental and dynamic 4-31G theoretical deformation densities. Contours as in Fig. 2(*a*).

non-bonding regions around both oxygen atoms. However, as observed in several other molecules, the lack of flexibility and polarization functions in the smaller basis set results in overestimation of the lone-pair peaks and insufficient density in the covalent-bond peaks.

The dynamic deformation density calculated from the extended-basis-set wavefunction using experimental rigid-body thermal parameters including all terms to a resolution of $\sin\theta/\lambda = 1{\cdot}2$ Å$^{-1}$ is plotted in Fig. 2(*a*). The sharper features of the deformation density including the lone-pair peaks and holes near the nuclei

are most affected by the combination of thermal smearing and series termination. A comparison of experimental and theoretical dynamic bond and lone-pair peak heights is given in Table 4. The differences noted between the extended basis set and 4-31G densities persist in the thermally smeared 4-31G deformation density plotted in Fig. 3(*a*). The bond peaks are lower and the lone-pair peaks higher than the extended-basis-set density. This trend is also evident in the comparison with experimental peak heights (Table 4). The overall agreement with experiment is much better for the extended-basis-set calculation.

A more detailed comparison with experiment is given in the double difference plots. The map of $\Delta(\Delta\rho)$ for the extended-basis-set calculation is plotted in Fig. 2(*b*) and the corresponding map for the 4-31G calculation in Fig. 3(*b*). The noise level in intermolecular regions is slightly more than expected from the estimate of 0·02 e/Å$^3$ for the experimental error at general positions. The large peaks at the edge of the maps arise from the water molecules present in the crystal lattice but neglected in the theoretical calculation. The differences between theory and experiment near the carbon and oxygen positions are not significant because of the large value of $\sigma(\Delta\rho)$ at those positions.

The double difference maps between the experimental and 4-31G theoretical deformation densities show a number of systematic and significant features. Positive differences are found in each of the covalent bonds indicating more density is present in the experimental maps than predicted by the theory, while in the lone-pair regions just the opposite result is found. Quite clearly the deficiencies previously observed in limited-basis-set calculations of the density also apply to thermally smeared densities. In the following analysis, therefore, only the densities obtained with the extended-basis-set calculation will be considered.

Table 4. *Comparison of bond and lone-pair peak heights in the dynamic deformation densities* (e/Å$^3$)

| | | Theory | |
|---|---|---|---|
| | Experiment | EBS | 4-31G |
| C(1)–C(1′) | 0·65 (3) | 0·58 | 0·38 |
| C(1)–O(1) | 0·38 (2) | 0·43 | 0·20 |
| C(1)–O(2) | 0·49 (2) | 0·62 | 0·46 |
| O(1)–H(1) | 0·27 (4) | 0·40 | 0·23 |
| O(1) l.p. | 0·42 (6) | 0·60 | 0·73 |
| O(2) l.p.1 | 0·50 (8) | 0·53 | 0·61 |
| O(2) l.p.2 | 0·38 (8) | 0·53 | 0·64 |

The experiment-extended basis-set $\Delta(\Delta\rho)$ map indicates generally excellent agreement between theory and experiment. There are some significant features which closely resemble features found in other comparisons of theory and experiment (Stevens, Rys & Coppens, 1977*a*, 1978). Each of the covalent-bond peaks is more elongated along the bond direction in the experimental density. Similar results for formamide (Stevens, Rys & Coppens, 1978) and sodium and potassium azide (Stevens, Rys & Coppens, 1977*a*,*b*) have been ascribed to insufficient flexibility in the bonding region remaining even in the extended basis set. More elongation of the bonding peaks is found, for example, in static Hartree–Fock densities of $N_2$ and NCCN (Hirshfeld, 1971). A contribution from the neglect of internal vibrational modes is also possible.

In the theoretical calculation, the effects of the intermolecular interactions between the molecule and the surrounding crystal have been ignored. The largest intermolecular interactions will result from the hydrogen bonds formed in the solid. A number of theoretical calculations (see for example Yamabe & Morokuma, 1975; Diercksen, 1971; Dreyfus, Maigret & Pullman, 1970; Kollman & Allen, 1970) have predicted some density changes throughout the molecule as a result of hydrogen-bond formation. The largest calculated change for long hydrogen bonds is an increase in the (static) density of the *X*—H bond of the donor by as much as 0·2 e/Å$^3$ (Dreyfus, Maigret & Pullman, 1970).

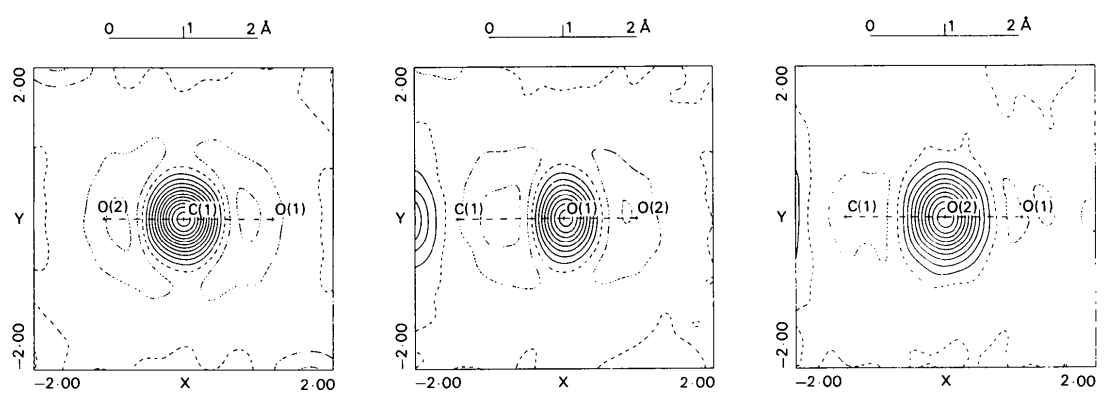


Fig. 4. Sections of the dynamic EBS theoretical density perpendicular to the bond axes at the bond midpoints. Contours as in Fig. 2(*a*). (*a*) C—C bond; (*b*) C—O bond; (*c*) C=O bond.

A peak of 0·4 (1) e/Å$^3$ is observed in the O(1)—H(1) bond of the $\Delta(\Delta\rho)$ map in qualitative agreement with the differences expected as a result of hydrogen bonding. The larger difference observed for oxalic acid may in part be due to the stronger interaction of the short [2·487 (1) Å] hydrogen bond.

Theoretical density differences due to hydrogen bonding also show some depletion of charge in the lone-pair regions around oxygen (Dreyfus, Maigret & Pullman, 1970; Yamabe & Morokuma, 1975). Larger differences [$\sim$−0·20 (8) e/Å$^3$] observed in the $\Delta(\Delta\rho)$ map are only marginally significant and may have other contributions as well.

In previous studies of formamide and the azide ion (Stevens, Rys & Coppens, 1977*a*, 1978), small differences between theoretical and experimental densities near the atomic centers but displaced off the bond axes have been attributed to electron correlation neglected in the theoretical calculations. This result is supported by calculations of the difference between

Table 5. *Maximum deviations of bond peaks from cylindrical symmetry* ($\rho_{L\neq0}$, e/Å$^3$) *and distance* ($r$, Å) *from center of bond*

| | Experiment | | Theory | |
|---|---|---|---|---|
| | $\rho_{L\neq0}$ | $r$ | $\rho_{L\neq0}$ | $r$ |
| C—C | 0·23 (2) | 0·45 | 0·09 | 0·64 |
| C—O | 0·19 (2) | 0·52 | 0·13 | 0·51 |
| C=O | 0·07 (2) | 0·49 | 0·10 | 0·57 |

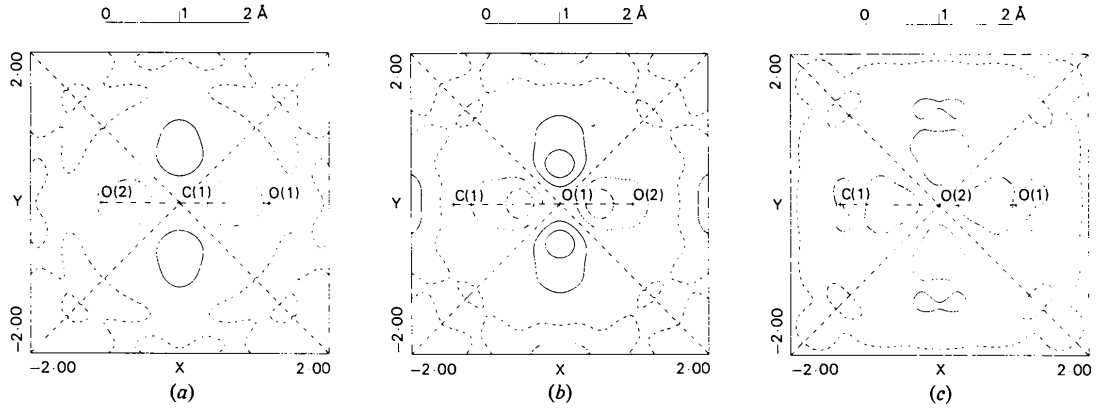


Fig. 5. Plots of the difference between sections of the dynamic EBS density perpendicular to the bond axis and the same plane rotated about the bond axis by 90°. Contours as in Fig. 2(*a*). (*a*) C—C bond; (*b*) C—O bond; (*c*) C=O bond.

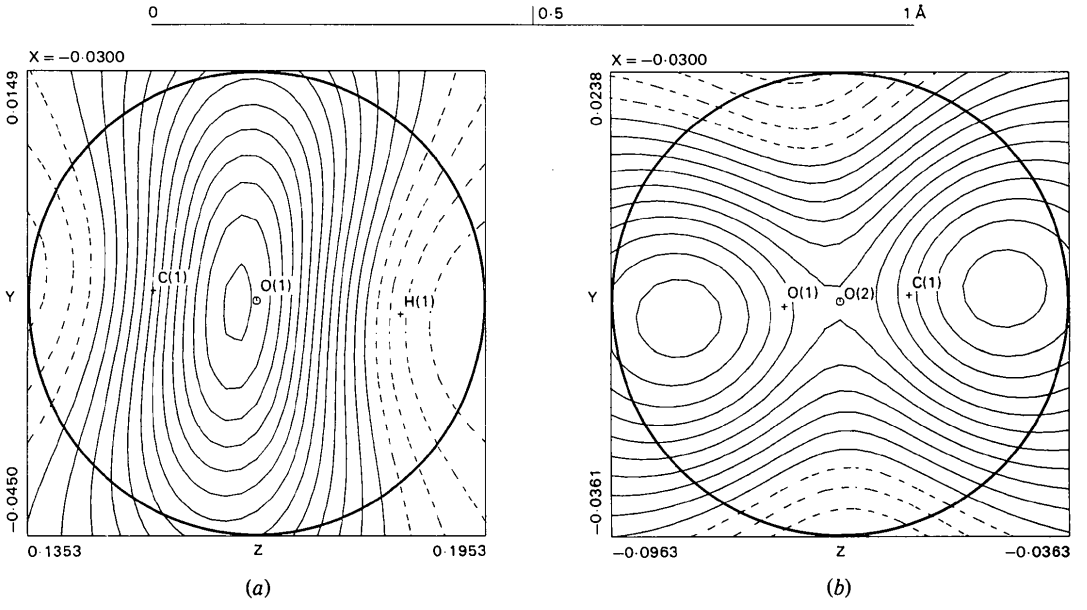


Fig. 6. Stereographic projection of the deformation density on the surface of a sphere with 0·3 Å radius and centered at the oxygen atom. Contours as in Fig. 2(*a*). (*a*) Projection of the hemisphere around O(1) onto the plane perpendicular to the line bisecting the H—O—C angle. (*b*) Projection of the hemisphere around O(2) and opposite the C=O bond onto the plane perpendicular to the bond.

densities corresponding to CI and Hartree–Fock wavefunctions for small molecules (Bader & Chandra, 1968; Smith, 1977; Bicerano, Marynick & Lipscomb, 1978). The size and location of these differences are generally in agreement with the $\Delta(\Delta\rho)$ map of oxalic acid, but since they are comparable in size to the level of experimental noise, a quantitative analysis must await more accurate experimental results.

Perpendicular sections of the thermally smeared theoretical densities through the midpoints of the C–C, C–O and C=O bonds are plotted in Fig. 4. As previously noted in both experimental (Coppens, Sabine, Delaplane & Ibers, 1969; Stevens & Coppens, 1980) and theoretical densities (Johansen, 1979), all three bonds are elongated perpendicular to the molecular plane. The deviations from cylindrical symmetry ($\rho_{L\neq 0}$) for the three bonds are plotted Fig. 5 and the maximum deviations listed in Table 5. As in the experiment, a larger deviation is found for the C–O bond than for the formally double C=O bond. The C–C bond, however, shows less $\pi$ character than found in the experimental density.

Stereographic projections of the dynamic deformation in the lone-pair region around O(1) and O(2) are plotted in Fig. 6. The projection around O(2) shows two maxima in the molecular plane consistent with $sp^2$ hybridization and in excellent agreement with the experiment (Stevens & Coppens, 1980). Projection of the density about O(1) gives a single peak with maximum in the molecular plane but highly elongated perpendicular to the plane. This is not in agreement with the experimental density which shows much less elongation. Two peaks are found in the static density and in the density calculated by Johansen (1979) indicating more $sp^3$ character in the (theoretical) O(1) lone-pair hybridization.

*Hydrogen bonds*

Theoretical calculations of the electron density distribution in hydrogen-bonded systems have been reported by several workers (Dreyfus & Pullman, 1970; Diercksen, 1971; Kollman & Allen, 1970; Yamabe & Morokuma, 1975). Commonly, the density is plotted as a difference between the hydrogen-bonded dimer and the sum of the isolated monomer densities. The deformation density, in which atomic rather than molecular densities are subtracted, has rarely been calculated for hydrogen bonds. Johansen (1979) has plotted both types of difference densities from calculations of the oxalic acid molecule acting as a donor to two water molecules. However, because of the size of the system it was necessary to use a smaller basis set than that used for the isolated molecule.

In order to investigate the density distribution in an intermediate hydrogen and compare this with the experimental results (Stevens & Coppens, 1980), the deformation density has been calculated from extended-basis wavefunctions of the water dimer, $(H_2O)_2$. The geometry was chosen to reproduce the dimensions of the short hydrogen bond as found in the structure of $\alpha$-oxalic acid dihydrate at 100 K (O···O distance = 2·487, O–H distance 1·071 Å). This geometry is therefore quite different from both the geometry of minimum energy and the experimental geometry of the isolated water dimer (Dyke & Muenter, 1974).

The (static) theoretical deformation density in the hydrogen bond of the water dimer is plotted in Fig. 7(*a*). In contrast to the corresponding experimental density [Fig. 6(*a*) of Stevens & Coppens (1980)], little deviation of the lone-pair peaks on the acceptor water molecule from the molecular mirror plane is observed. On the other hand, the deformation density calculated

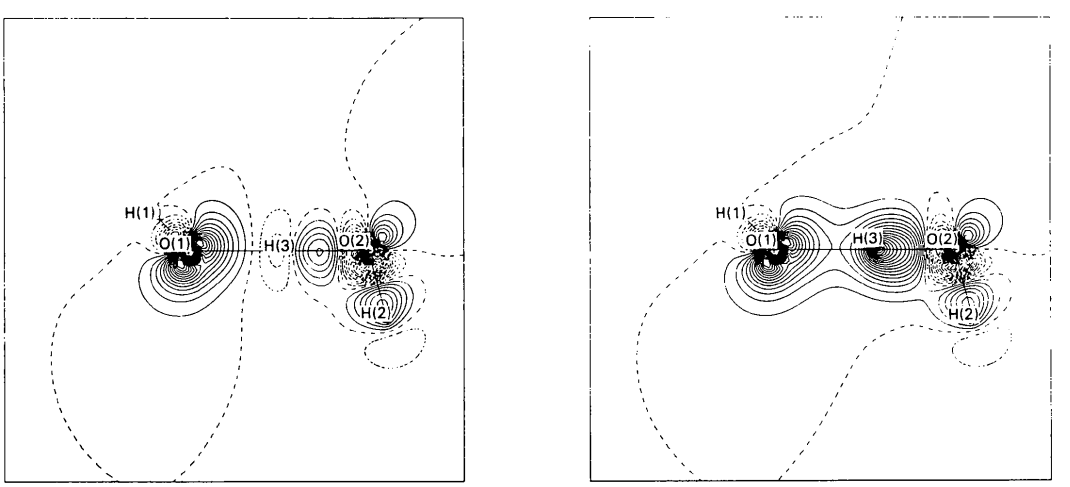


(*a*) (*b*)

Fig. 7. (*a*) Static EBS theoretical deformation density of the $(H_2O)_2$ dimer calculated in the plane containing the donor water molecule and bisecting the acceptor molecule. Contours as in Fig. 2(*a*). (*b*) Static deformation density as in (*a*) but without subtracting the density of the donor hydrogen atom.

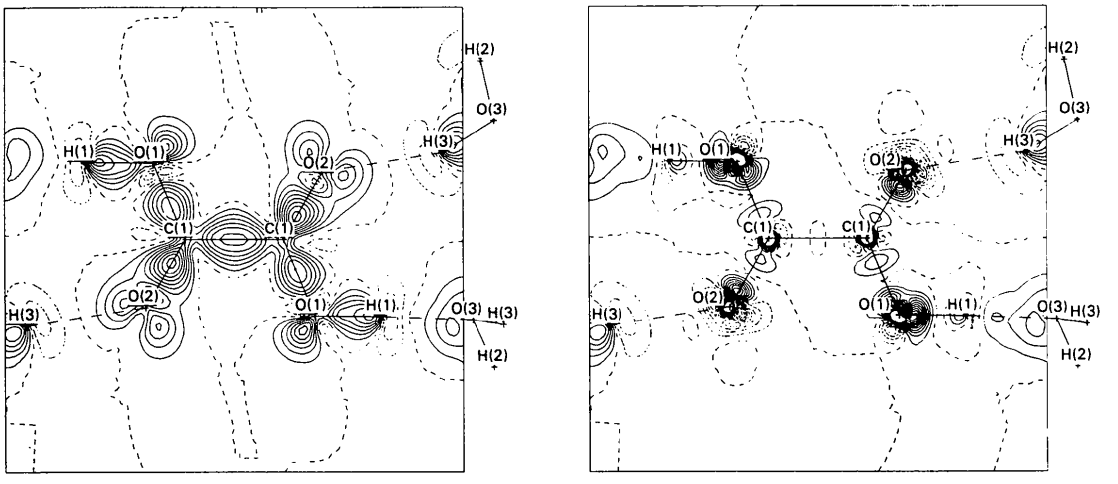


Fig. 8. (*a*) Experimental static model deformation density of the oxalic acid molecule. Contours as in Fig. 1(*a*). (*b*) Difference between experimental static model density and static EBS theoretical density. Contours as in Fig. 1(*a*).

without subtracting the hydrogen-atom density (Fig. 7*b*) is in good agreement with the experiment showing a ridge of density extending along the hydrogen bond between donor and acceptor with a saddle point of 0·28 e/Å$^3$. The expected reduction in the height of the ridge due to thermal smearing will probably be offset by the higher proton-donating ability of oxalic acid relative to the water molecule. The agreement between theoretical and experimental deformation densities in the short hydrogen bond is therefore very good.

Table 6. *Comparison of bond and lone-pair peak heights in the static deformation densities*

| | Experiment | EBS | Theory 4-31G | Johansen (1979) |
|---|---|---|---|---|
| C(1)–C(1) | 0·64 | 0·67 | 0·40 | 0·8 |
| C(1)–O(1) | 0·60 | 0·54 | 0·25 | 0·6 |
| C(1)–O(2) | 0·85 | 0·70 | 0·54 | 0·8 |
| O(1)–H(1) | 0·65 | 0·56 | 0·34 | 0·6 |
| O(1) l.p.1 | 0·66 | 1·10 | 1·18 | 1·0 |
| O(2) l.p.1 | 0·42 | 1·22 | 1·49 | 1·2 |
| O(2) l.p.2 | 0·41 | 1·32 | 1·39 | 1·2 |

*Comparison of static densities*

An alternative to comparing experimental densities with smeared densities is deconvolution of thermal motion from the experimental distribution. Since information on the static density is lost in the experiment due both to thermal smearing and the limited resolution of the experiment, deconvolution using model density functions substitutes the features of the model for the lost information. Also, the estimated error distribution in the experimental static density is more difficult to evaluate (Coppens & Stevens, 1977).

The requirements of a valid deconvolution have been discussed by Hirshfeld (1977*a*). Obviously, the model must be sufficiently flexible to fit all of the features of the static density. Multipole refinements of the theoretical structure factors of formamide (Stevens, Rys & Coppens, 1978; Stevens, 1979) show that both the multipole expansion used here (Hansen & Coppens, 1978) and the non-orthogonal expansion used by Hirshfeld (1977*b*) satisfy this requirement.

The static model deformation density of the oxalic acid molecule calculated from the refined multipole populations (Stevens & Coppens, 1980) is plotted in Fig. 8(*a*). While no error distribution has been calculated, it may be assumed that, as with the smeared density, features within about 0·3 Å of the atomic nuclei are not significant. A comparison of the model peak heights with values from the static theoretical densities is given in Table 6. The most obvious difference between the model and the theoretical results is in the low peak heights obtained for the oxygen non-bonding density. In other areas, the agreement is generally very good.

The agreement between theory and experiment is displayed in detail in the static double-difference density plotted in Fig. 8(*b*). As with the dynamic density, the features near the edges of the map are due to the water molecules, neglected in the theoretical calculation. As noted in the peak heights, the lone-pair features are much lower in the experimental density which results in large holes at these positions in $\Delta(\Delta\rho)$. There are large peaks in $\Delta(\Delta\rho)$ at each of the carbon and oxygen sites due to the sharp negative holes in the static theoretical density which are not reproduced in the experiment. In the bonding regions, the agreement

Table 7. *Comparison of bond distances* (Å) *and angles* (°) *in the gaseous and solid state*

| | Crystal (100 K)[a] | Gas[b] |
|---|---|---|
| C–C | 1·544 (1) | 1·548 (4) |
| C–O | 1·287 (1) | 1·339 (2) |
| C=O | 1·222 (1) | 1·208 (1) |
| O–H | 1·071 (1) | 1·056 (14)[c] |
| C–C=O | 120·41 (5) | 123·1 (9) |
| O–C=O | 127·02 (5) | 125·0 (2) |
| C–O–H | 113·3 (1) | 104·4 (23)[c] |

(*a*) Stevens & Coppens (1980). (*b*) Náhlovská, Náhlovský & Strand (1970). (*c*) An intramolecular hydrogen bond is formed in the gas phase.

is much better, although there is again evidence that the experimental bond peaks are more elongated along the bond axes than the theoretical densities.

Refinement of multipole density functions from X-ray diffraction data has several advantages. The model-fitting process acts as a filter for random experimental noise. The multipole functions give a description of the density in terms of a small number of analytic functions and facilitate the calculation of other properties of the charge density. However, the ability of multipole refinements to deconvolute thermal motion properly and yield reliable static densities has not been extensively tested.

Comparison of the dynamic and static multipole model densities reveals a tendency of the static density not to contain any features which are sharper than those present in the dynamic density. Examples of such features are the sharp holes near the atomic centers and lone-pair peaks which are present in static theoretical densities but not observed in the experimental model density. These are, of course, the features for which complete information is not available in the experiment because of limited experimental resolution and thermal smearing. A similar effect has been noted in the behavior of dynamic model densities on increasing resolution (Hansen & Coppens, 1978). For other features of the density, the comparison of static multipole model densities and theoretical densities yields essentially the same information as the comparison of dynamic densities.

Clearly, more studies of deconvolution techniques and the propagation of both random and systematic errors in the static density are desirable. Meanwhile, static multipole densities must be interpreted with caution.

## Discussion

One of the largest contributions to the discrepancies between the experimental deformation densities and thermally smeared theoretical density for the oxalic acid molecule is the neglect of intermolecular interactions. In crystals of α-oxalic acid dihydrate, the dominant intermolecular interaction is hydrogen bonding. The magnitude of this interaction is evident in the change in molecular geometry between the gas and solid phase (Table 7). Compared with the results of electron diffraction (Náhlovská, Náhlovský & Strand, 1970), the C–O bond length decreases by 0·052 Å while the C=O bond length increases by 0·014 Å when the compound is solid. This change in geometry is very similar to the decrease in C–N bond length and increase in C=O bond length observed for the formamide molecule (Stevens, Rys & Coppens, 1978), and indicates an increase in $\pi$ delocalization in the solid.

The increased delocalization in the oxalic acid molecule is also evident in the increased $\pi$ character of the experimental C–C and C–O bond densities compared with the theoretical calculation (Fig. 4, Table 5). This is also in agreement with the differences between theory and experiment observed in the lone-pair density at O(1). While the theoretical density is quite elongated perpendicular to the plane, the experimental density is less extended indicating a change in hybridization toward the $(1s)^2(2sp^2)^1$-$2(sp^2)^1(2sp^2)^2(2p\pi)^2$ scheme proposed by Coppens, Sabine, Delaplane & Ibers (1969).

The calculated density distribution in the water dimer is qualitatively in agreement with the experimental density distribution observed in the short hydrogen bond of oxalic acid dihydrate. In oxalic acid, the donor proton is obviously more acidic than in the water dimer, which is likely to be responsible for the lower valence density obtained from the theoretical calculation along the hydrogen bond and also the lack of significant perturbation of the lone-pair density calculated for the acceptor water molecule.

The remaining discrepancies between the experimental and smeared theoretical densities are small but consistent with those observed in previous comparisons (Stevens, Rys & Coppens, 1977*a*, 1978). These differences are attributed to the neglect of internal modes in the thermal smearing, remaining basis-set truncation effects and the neglect of thermal smearing. Since these effects can in principal be evaluated theoretically, more studies of them are clearly necessary as a result of the improving accuracy of experimental density distributions.

Comparison of both static and dynamic theoretical densities calculated with the 4-31G and extended basis sets reveals the tendency of 4-31G calculations to overestimate lone-pair features and underestimate bond peaks in the deformation density. The experimental density is in better agreement with the extended-basis-set calculation and the current level of experimental accuracy is certainly sufficient to discriminate between calculated densities. Densities calculated with

wavefunctions of 4-31G quality must therefore be considered useful only for qualitative comparisons with experiment.

Support of this work by the National Science Foundation under Grants CHE 76-13342 and CHE 76-21995 is gratefully acknowledged. The author is indebted to Dr J. Rys for assistance with some of the calculations and to Dr P. Coppens for many helpful discussions.

### References


BADER, R. F. W. (1975). *MTP International Review of Science, Physical Chemistry, Series* 2, Vol. 1, p. 43–78. London: Butterworths.

BADER, R. F. W. & CHANDRA, A. K. (1968). *Can. J. Chem.* **46**, 953–966.

BICERANO, J., MARYNICK, D. S. & LIPSCOMB, W. N. (1978). *J. Am. Chem. Soc.* **100**, 732–739.

CADE, P. E. (1972). *Trans. Am. Crystallogr. Assoc.* **8**, 1–36.

COPPENS, P. & SABINE, T. M. (1969). *Acta Cryst.* B**25**, 2441–2451.

COPPENS, P., SABINE, T. M., DELAPLANE, R. G. & IBERS, J. A. (1969). *Acta Cryst.* B**25**, 2451–2458.

COPPENS, P. & STEVENS, E. D. (1977). *Isr. J. Chem.* **16**, 175–179.

DIERCKSEN, G. H. R. (1971). *Theor. Chim. Acta*, **21**, 335–367.

DIETRICH, H. & SCHERINGER, C. (1978). *Acta Cryst.* B**34**, 54–63.

DITCHFIELD, R., HEHRE, W. J. & POPLE, J. A. (1971). *J. Chem. Phys.* **54**, 724–728.

DREYFUS, M., MAIGRET, B. & PULLMAN, A. (1970). *Theor. Chim. Acta*, **17**, 109–119.

DREYFUS, M. & PULLMAN, A. (1970). *Theor. Chim. Acta*, **19**, 20–37.

DUPUIS, M. & KING, H. F. (1977). *Int. J. Quantum Chem.* **11**, 613–625.

DUPUIS, M., RYS, J. & KING, H. F. (1976). *J. Chem. Phys.* **65**, 111–116.

DYKE, T. R. & MUENTER, J. S. (1974). *J. Chem. Phys.* **60**, 2929–2930.

FELD, R. & LEHMANN, M. S. (1979). Unpublished results.

HANSEN, N. K. & COPPENS, P. (1978). *Acta Cryst.* A**34**, 909–921.

HASE, H. L., REITZ, H. & SCHWEIG, A. (1976). *Chem. Phys. Lett.* **39**, 157–159.

HASE, H. L., SCHULTE, K. W. & SCHWEIG, A. (1977). *Angew. Chem. Int. Ed. Engl.* **89**, 257–258.

HELMHOLDT, R. B. & VOS, A. (1977). *Acta Cryst.* A**33**, 456–465.

HIRSHFELD, F. L. (1971). *Acta Cryst.* B**27**, 769–781.

HIRSHFELD, F. L. (1977*a*). *Isr. J. Chem.* **16**, 168–174.

HIRSHFELD, F. L. (1977*b*). *Isr. J. Chem.* **16**, 226–229.

IRNGARTINGER, H., HASE, H. L., SCHULTE, K. W. & SCHWEIG, A. (1977). *Angew. Chem. Int. Ed. Engl.* **89**, 187.

JOHANSEN, H. (1979). *Acta Cryst.* A**35**, 319–325.

KOLLMAN, P. A. & ALLEN, L. C. (1970). *J. Chem. Phys.* **52**, 5085–5094.

NÁHLOVSKÁ, Z., NÁHLOVSKÝ, B. & STRAND, T. G. (1970). *Acta Chem. Scand.* **24**, 2617–2628.

POPLE, J. A. & BINKLEY, J. S. (1975). *Mol. Phys.* **29**, 599–611.

ROOS, B., SALEZ, C., VIELLARD, A. & CLEMENTI, E. (1968). *IBM Res. Rep.* RJ518.

ROOTHAAN, C. C. J. (1951). *Rev. Mod. Phys.* **23**, 69–89.

SCHERINGER, C., KUTOGLU, A., HELLNER, E., HASE, H. L., SCHULTE, K. W. & SCHWEIG, A. (1978). *Acta Cryst.* B**34**, 2162–2165.

SCHERINGER, C., MULLEN, D. & HELLNER, E. (1978). A**34**, 621–625.

SCHOMAKER, V. & TRUEBLOOD, K. N. (1968). *Acta Cryst.* B**24**, 63–76.

SMITH, V. H. (1977). *Phys. Scr.* **15**, 147–162.

STEVENS, E. D. (1979). Unpublished results.

STEVENS, E. D. & COPPENS, P. (1980). *Acta Cryst.* B**36**, 1864–1876.

STEVENS, E. D., RYS, J. & COPPENS, P. (1977*a*). *J. Am. Chem. Soc.* **99**, 265–267.

STEVENS, E. D., RYS, J. & COPPENS, P. (1977*b*). *Acta Cryst.* A**33**, 333–338.

STEVENS, E. D., RYS, J. & COPPENS, P. (1978). *J. Am. Chem. Soc.* **100**, 2324–2328.

YAMABE, S. & MOROKUMA, K. (1975). *J. Am. Chem. Soc.* **97**, 4458–4465.